Nonlinear modal interaction analysis and vibration characteristics of a Francis hydro-turbine generator unit

Beibei Xu[a,b], Xingqi Luo[*,c], Mònica Egusquiza[d], Wei Ye [a,b], Jing Liu[a,b], Eduard Egusquiza[d], Diyi Chen[*a,b], Pengcheng Guo[c]

[a]*Institute of Water Resources and Hydropower Research, Northwest A&F University, Shaanxi Yangling 712100, P. R. China*
[b]*Key Laboratory of Agricultural Soil and Water Engineering in Arid and Semiarid Areas, Ministry of Education, Northwest A & F University, Shaanxi Yangling 712100, P. R. China*
[c]*State Key Laboratory Based of Eco-hydraulic Engineering in Arid Area, Xi'an University of Technology, Xi'an 710048, Shaanxi, P. R. China*
[d]*Center for Industrial Diagnostics and Fluid Dynamics (CDIF), Polytechnic University of Catalonia (UPC), Av. Diagonal, 647, ETSEIB, 08028 Barcelona, Spain.*

***Corresponding author: Xingqi Luo, Diyi Chen**
Mailing Address: Institute of Water Resources and Hydropower Research, Northwest A&F University, Shaanxi Yangling 712100, China
Telephones: 086-181-6198-0277
E-mail: xingqiluo@126.com；diyichen@nwsuaf.edu.cn

Abstract: The Francis hydro-turbine generator unit (FHTGU) is a typical nonlinear system with the coupling hydraulic, mechanical and electric subsystems. It is a challenge to understand the reasons for its operational failures because the major reason for failures involves complex interactions of the three subsystems. Subsystems' model interaction with the method of normal forms has been well developed and investigated, overcoming the linear methods used in the FHTGU's stability analysis. However, these methods have not to quantify higher-order terms in a mathematically accurate type to capture dynamic modal interactions between subsystems. Due to the accelerating expansion of hydropower stations, stability of FHTGU shows singular nonlinear oscillations and new methods have to be upgraded to cope with this new situation. In this study, the nonlinear modal method is introduced to analyze the dynamic modal interactions between subsystems, and results given by the different methods are compared to verify the method's feasibility. The effect of the second order modes is quantified to investigate its effect on the dynamic characteristics of FHTGU, and the vibration characteristics affected by the wind generation system are also investigated. The result shows that the intensity of modes can be effectively reduced to satisfy the stable requirements. All of these results provide a theoretical guidance for the stable operation of FHTGUs.

Key words: Nonlinear modal method; Francis hydro-turbine generator unit; interaction effect; vibration characteristics; stability

1 Introduction

The Francis hydro-turbine generator unit (FHTGU) is a highly nonlinear dynamic system affected by the dynamic characteristics of subsystems such as the whole passage (penstock, volute and draft tube), hydraulic turbine, generator, etc [1]. The time domain simulation method is a general method used to describe the nonlinear dynamic behavior of FHTGU, which is based on the numerical simulation to simulate the operation characteristics under certain disturbances [2-4]. Using this method, the nonlinear properties of the system are fully investigated using the nonlinear differential algebraic equations as a mathematical model, but it is difficult to explain the essence of the complex dynamic characteristics of FHTGU directly. In addition, these methods have not to quantify higher-order terms in a mathematically accurate type to capture the dynamic modal interactions between subsystems [5-7]. Therefore, it is necessary to explore a new method to quantify the interaction effects of subsystems. The modal series theory proposed by Pariz. et al is used to explore the internal nature of the complex high-dimensional nonlinear system by quantifying the effects of state variables. It is widely used in engineering projects. Pariz. et al first proposed the modal series method for applying to complex nonlinear systems [8]. The modal series theory directly explain the internal nature of complex dynamic characteristics of the system by quantifying the effect of state variables. The fundamental principle of this method is based on the Taylor series expansion and the linear transformation of the state space to obtain the second order approximate analytical solution of the nonlinear system [9-11]. This method is characterized by easy derivation, simple calculation and obtaining the analytical solutions without solving high-dimensional nonlinear equations, and it is widely used to analyze the interaction effect of power systems with faults or disturbances [12-14]. For example, Khatibi et al. utilized a modified modal series to investigate weakly nonlinear circuits using a modified modal series [12]. Sajjadi et al. described a new off-line nonlinear model predictive control approach for continuous-time affine-input nonlinear systems using an extended modal series method [13]. Based on the modal series expansion method, various sound models for predicting transmission loss of compressor mufflers are compared by Li et al. [14]. Jajarmi et al. presented an efficient parallel processing approach for solving the optimal control problem of nonlinear composite systems [15]. Naghshbandy et al. analyze fault location effect on the inter-area oscillations in stressed power systems by modal series method [16]. To the author’s best knowledge, most of the scholars mainly focused on utilizing the modal series method to study the characteristics of system’s component, such as control system, rather than FHTGU [17-20]. However, as the key component of the power system, the dynamic properties of FHTGU significantly influences the stable and safe operation of power system. Therefore, this paper devotes to investigate the interaction analysis of FHTGU.

Motivated by the above discussion, there are three advantages which make this approach more attractive compared with the prior work. First, a mathematical model of the shafting system is established by considering the hydraulic unbalanced force. Second, the linear related action of the shafting system is analyzed in detail through eigenvalue analysis and participation factor analysis. Third, the vibration characteristics of FHTGU are investigated by utilizing nonlinear interaction indices.

The rest of this study is organized as follows. In Section 2, the model of FHTGU is obtained, and the modal series method is proposed. Section 3 studies the interaction effects by analyzing eigenvalue and participation factor. Section 4 closes this paper.

2 Mathematical Model

2.1 Model of the Francis hydro-turbine generator unit

The FHTGU consists of the upper guide bearing, lower guide bearing, water guide bearing, generator rotor and hydro-turbine runner [21]. Considering the lateral vibration and neglecting the influence of thrust bearing and shaft on the vibration of the FHTGU, the kinetic energy (*T*) and potential energy (*U*) of the FHTGU is [22]

$$\begin{cases} T=\dfrac{1}{2}(J_1+m_1e_1^2)\varphi^2+\dfrac{1}{2}\left[J_1+m_2\left(r^2+e_2^2\right)\right]\theta^2+\dfrac{1}{2}m_1(\dot{x}_{01}^2+\dot{y}_{01}^2+e_1^2\dot{\varphi}^2-2\dot{x}_{01}e_1\dot{\varphi}\sin\varphi+2\dot{y}_{01}e_1\dot{\varphi}\cos\varphi) \\ \quad+\dfrac{1}{2}m_2(\dot{x}_{02}^2+\dot{y}_{02}^2+e_2^2\dot{\varphi}^2-2\dot{x}_{02}e_2\dot{\varphi}\sin\varphi+2\dot{y}_{02}e_2\dot{\varphi}\cos\varphi) \\ U=\dfrac{1}{2}k_1\left(x_{01}^2+y_{01}^2\right)+\dfrac{1}{2}k_2\left(x_{01}^2+y_{01}^2+2rx_{01}\cos\theta+2ry_{01}\sin\theta+r^2\right) \end{cases}, \tag{1}$$

where m_1 and m_2 are the mass of the generator rotor and the mass of hydro-turbine runner, respectively. J_1 and J_2 are the moment inertia of generator rotor and hydro-turbine runner, respectively. k_1 and k_2 are the bearing stiffness of the generator rotor and hydro-turbine runner, respectively. e_1 and e_2 are the offset of the generator rotor and hydro-turbine runner, respectively. x_{01} and y_{01} are the centroid deviation of the generator rotor in *x*-axis and *y*-axis, respectively. x_{02} and y_{02} are the centroid deviation of the hydro-turbine runner in *x*-axis and *y*-axis, respectively. φ and θ are the phase of the generator rotor and hydro-turbine runner, respectively. *r* is the distance between the centroid of rotor and runner. The Lagrange function is defined as the difference between kinetic energy and potential energy, which is

$$L=T-U\ . \tag{2}$$

Based on the Lagrange function, the model of FHTGU is obtained as

$$\begin{cases} \dfrac{d}{dt}\left(\dfrac{\partial L}{\partial \dot{x}_{01}}\right)-\dfrac{\partial L}{\partial x_{01}}=\Sigma F_x \\ \dfrac{d}{dt}\left(\dfrac{\partial L}{\partial \dot{y}_{01}}\right)-\dfrac{\partial L}{\partial \mathrm{y}_{01}}=\Sigma F_y \end{cases}, \tag{3}$$

where F_x and F_y are the forces acting on the FHTGU (see Tab. 1).

Tab. 1 Forces acting on different parts of the shafting system of a hydro-turbine generator unit.

Part	Rub impact	Oil-film force	Damping force	Asymmetric magnetic pull	Unbalanced hydraulic force
Bearing		√, ref. [28]			
Rotor	√, ref. [23]		√, ref. [23]	√, ref. [28]	
Turbine runner			√		see Supplementary note

In light of the above analysis, the model of FHTGU is further developed as

$$\begin{cases} \left(m_1+m_2\right)\ddot{x}_{01}-\left[\left(m_1e_1+m_2e_2\right)\sin\varphi+m_2r\sin\theta\right]\dot{\omega}-\left[\left(m_1e_1+m_2e_2\right)\cos\varphi+m_2r\cos\theta\right]\omega^2-\left(k_1+k_2\right)x_{01}+k_2r\cos\theta=\sum F_x \\ \left(m_1+m_2\right)\ddot{y}_{01}+\left[\left(m_1e_1+m_2e_2\right)\cos\varphi+m_2r\cos\theta\right]\dot{\omega}-\left[\left(m_1e_1+m_2e_2\right)\sin\varphi+m_2r\sin\theta\right]\omega^2+\left(k_1+k_2\right)y_{01}+k_2r\sin\theta=\sum F_y \end{cases}. \tag{4}$$

2.2 The modal series method

The modal series method, as a novel approach in its application for nonlinear systems, and as an alternative technique to obtain closed solutions from response of nonlinear systems, has some unique aspects which can distinguish it from other approximate methods [24, 25]. The direct calculation of high-order nonlinear equations is avoided by this method of solution. This method does not employ nonlinear transformation and does not suffer from resonance condition. Hence, the modal series theory is used to study the dynamic behaviors of FHTGU.

With respect to nonlinear dynamic systems, eigenvalues λ_1, λ_2,…, λ_N are defined as the linear modes. Due to the sophisticatedly nonlinear and strongly coupled of nonlinear dynamic systems, these linear modes interact to each other, which excite many interactive modes, such as $i_1\lambda_1+i_2\lambda_2+\ldots+i_N\lambda_N$ (Details see ref. [12]). Parameters Y_0 and $h2^j_{kl}$ make the most contributions to these interactive modes. Parameter Y_0 is the disturbance quantization and used to investigate the disturbance effect on the dynamic stability of the nonlinear systems. Parameter $h2^j_{kl}$ contains the nonlinear parts of the internal structure of the original system, describing the strength of nonlinear related action between mode j and composite modes (k, l) (Details see ref. [14]).

The second order modal time response term $K^i_{kl}e^{(\lambda_k+\lambda_l)t}$ is affected by two parameters, which are amplitude K^i_{kl} and time constant $T_{kl}=-1/real(\lambda_k+\lambda_l)$. The amplitude K^i_{kl} includes these two parameters, i.e., Y_0 and $h2^j_{kl}$. Based on this, the second order nonlinear interaction index is written as

$$I2^i_{kl}=\left|\frac{K^i_{kl}}{real\left(\lambda_k+\lambda_l\right)}\right| \quad i=1,2,\ldots,5\,. \tag{5}$$

To analyze the dynamic characteristics of FHTGU by nonlinear modal series method, it is necessary to determine the interaction strength between modes and state variables. Here, the participation factor is selected to evaluate the interaction strength between modes and state variables.

Assuming that only the state variable x_i is disturbed with its amplitude of 1, and the initial values of other state variables are 0, the initial value of FHTGU is represented as

$$Y_0=VX_0=\begin{bmatrix} v_{1i}\\ v_{2i}\\ v_{3i}\\ v_{4i}\\ v_{5i}\end{bmatrix},\quad y_{j0}=v_{ji}\,. \tag{6}$$

Hereby, the solution of the nonlinear system is written as

$$\begin{aligned} x_i(t)=&\sum_{j=1}^{5}u_{ij}\left(v_{ji}-\left\{\sum_{k=1}^{5}\sum_{l=1}^{5}h2^j_{kl}v_{ki}v_{li}\right\}_{(k,l,j)\notin R_2'}\right)e^{\lambda_j t}\\ &+\sum_{j=1}^{5}u_{ij}\left\{\sum_{k=1}^{5}\sum_{l=1}^{5}h2^j_{kl}v_{ki}v_{li}e^{(\lambda_k+\lambda_l)t}\right\}_{(k,l,j)\notin R_2'}\\ &+\left\{\sum_{j=1}^{5}\left(\sum_{k=1}^{5}\sum_{l=1}^{5}u_{ij}C^j_{kl}v_{ki}v_{li}\right)te^{\lambda_j t}\right\}_{(k,l,j)\in R_2'} \end{aligned}. \tag{7}$$

The nonlinear participation factor of i-th state variable in the j-th oscillation mode is expressed as

$$P2_{ij}=u_{ij}\left(v_{ji}-\left\{\sum_{k=1}^{5}\sum_{l=1}^{5}h2^j_{kl}v_{ki}v_{li}\right\}\right)_{(k,l,j)\notin R_2'}, \tag{8}$$

where the first term ($\left(u_{ij}v_{ji}\right)_{(k,l,j)\notin R_2'}$

term ($\sum_{k=1}^{5}\sum_{l=1}^{5} h2_{kl}^{j} v_{ki} v_{li} \quad {}_{(k,l,j)\notin R_2'}$) is the nonlinear correction term for the linear interaction.

2.3 Coupling FHTGU with the hydro-turbine governing system in a hybrid power system

The FHTGU is coupled with the hydro-turbine governing system. The hydro-turbine governing system consists of the PID control subsystem and the hydro-mechanical subsystem. The PID control subsystem belongs to a linear controller, which forms a control deviation between the reference value and the output value on the basis of the proportional-integral-differential loop to enable the frequency regulation. Generally, the mechanism of the PID control subsystem is expressed as:

$$\begin{cases} K_P = (\mathrm{T_d} + \mathrm{T_n}) / (\mathrm{b_t T_d}) \approx 1/\mathrm{b_t} \\ K_i = 1/(\mathrm{b_t T_d}) \\ K_D = T_n / b_t \end{cases} , \tag{9}$$

where K_p, K_i and K_D are the proportional, the integral, and the differential adjustment coefficient, respectively. T_n, T_d and b_t are the acceleration time constant, the buffer time constant and the transient difference coefficient, respectively. Thus, the schematic diagram of the PID control subsystem is shown in Fig. 1.

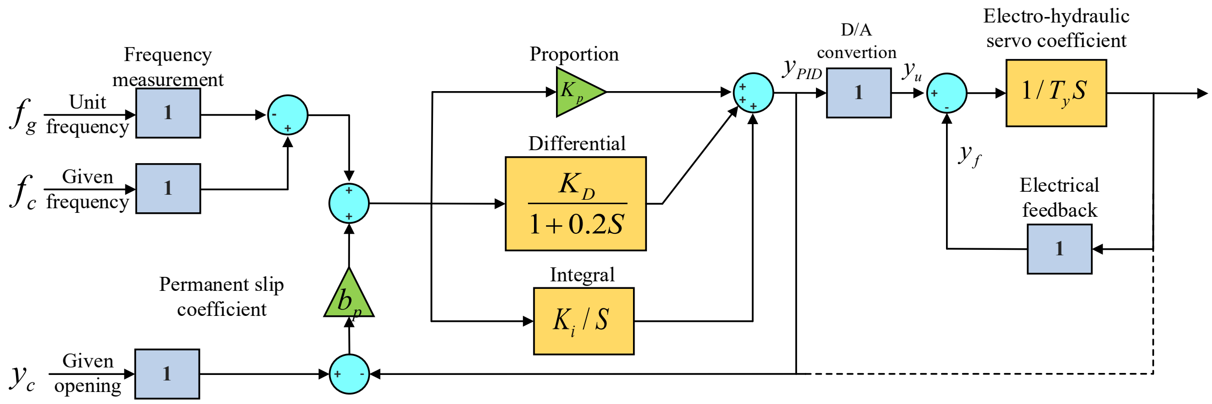

Fig. 1 Transfer function of the PID control subsystem. Parameters K_p, K_i and K_D represent the proportional-integral-differential loop, and parameters b_p, y and T_y represent the difference coefficient, the guide vane opening and the relay time constant, respectively.

The hydro-mechanical subsystem governs the hydraulic servomotor, which essentially belongs to an integral loop. The regulating performance of the hydro-mechanical subsystem is described by the start time and stop time of the hydraulic servomotor. A conventional hydro-mechanical subsystem is expressed by the transfer functions, as shown in Fig. 2.

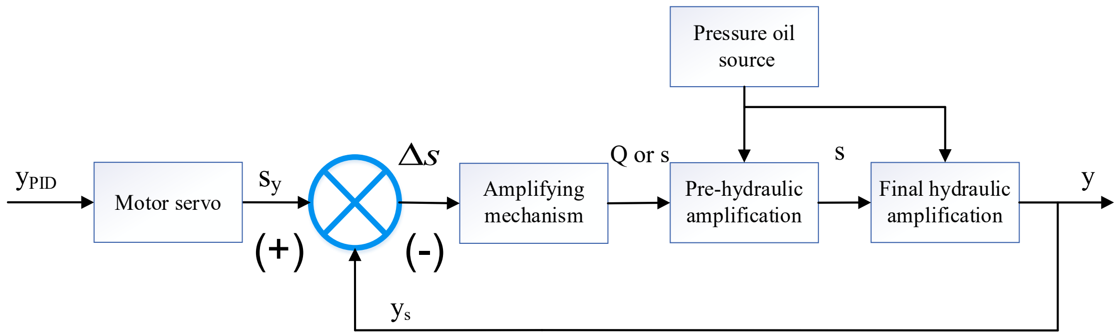

Fig. 2 Transfer function of the hydro-mechanical subsystem defined by the transfer functions. Parameters y_{PID}, s_y, y_s and y represent the microcomputer regulator output signal, the feedback signal,

the mechanical displacement signal and the guide vane opening.

There are two dynamic performance patterns that could reflect the characteristic of the penstock flow, i.e., the rigid water hammer and the elastic water hammer. Comparing the rigid pattern, the elastic water hammer is better to describe the actual motion of the penstock flow. Thus, the transfer function of the penstock ($G_D(s)$) is expressed as:

$$\begin{cases} G_D(s) = \dfrac{\overline{h}_q(s)}{\overline{q}(s)} = \dfrac{b_3 s^3 + b_2 s^2 + b_1 s + b_0}{a_2 s^2 + a_1 s + a_0} \\ a_0 = 24h_\omega;\ a_1 = 6T_r h_f;\ a_2 = 3T_r^{\,2} h_\omega \\ b_0 = -24T_r h_\omega h_f;\ b_1 = -24T_r h_\omega^{\,2};\ b_2 = -3T_r^{\,2} h_\omega h_f;\ b_3 = -T_r^{\,3} h_\omega^{\,2} \\ \end{cases}$$

$\overline{h}q$ $\overline{q}$

Based on Eq. (10), the characteristic of the hydro-turbine is obtained as:

$$\begin{cases} q = q_0 + \overline{q} = a_2 x_3 + a_1 x_2 + a_0 x_1 + q_0 \\ h_q = 1 - h_{fc} - h = 1 - f_p q^2 - \dfrac{q^2}{y^2} \end{cases}$$

where q_0 and h_{fc} are the relative initial flow and the water head loss coefficient.

The rotor motion equation for the hydraulic generator is written as:

$$\begin{cases} 2H\dfrac{d\omega}{dt} = P_{mac} - P_e - K_D \Delta\omega \\ \dfrac{d\theta}{dt} = \omega_b \omega \end{cases}$$

where P_{mac} is the mechanical power of generator rotor, P_e is the electromagnetic power, H is the inertia constant, K_D is the damping coefficient, ω is the generator rotor speed, ω_b is the reference value of the generator rotor speed, and θ is the rotor angle, respectively.

The electromagnetic equation of the generator is expressed as:

$$\begin{cases} e_d = X_q iq - Ri_d \\ T'_{d0}\dfrac{dE'_q}{dt} = E_f - E'_q - (X_d - X'_d)i_{\mathrm{d}} \\ e_q = E'_q - X'_d i_d - Ri_q \end{cases}$$

where $T'_{d0}$is the open-circuit transient time constant in d-axis, E'_q is the transient electromotance in q-axis, E_f is the excitation potential of rotor, and X'_d is the transient reactance in d-axis, respectively. X_d and X_q are the synchronous reactances in d-axis and q-axis, respectively. i_d and i_q are the output currents in d-axis and q-axis, respectively. e_d and e_q are the terminal voltages in d-axis and q-axis, respectively.

The whole system of the FHTGU and the governing system is used to link the node 1 of the typical IEEE 9-node system. Nodes 2 and 3 are linked with a wind power generation system and a power gird with voltage level of 330 kV, respectively. To facilitate the research, all nodes and load parameters of the line are taken the same value. Detail parameter values see Ref. [29]. To reduce the influence of the line loss, the line length is taken a smaller value of 10 km. The established model of the hybrid power system is shown in Fig. 3.

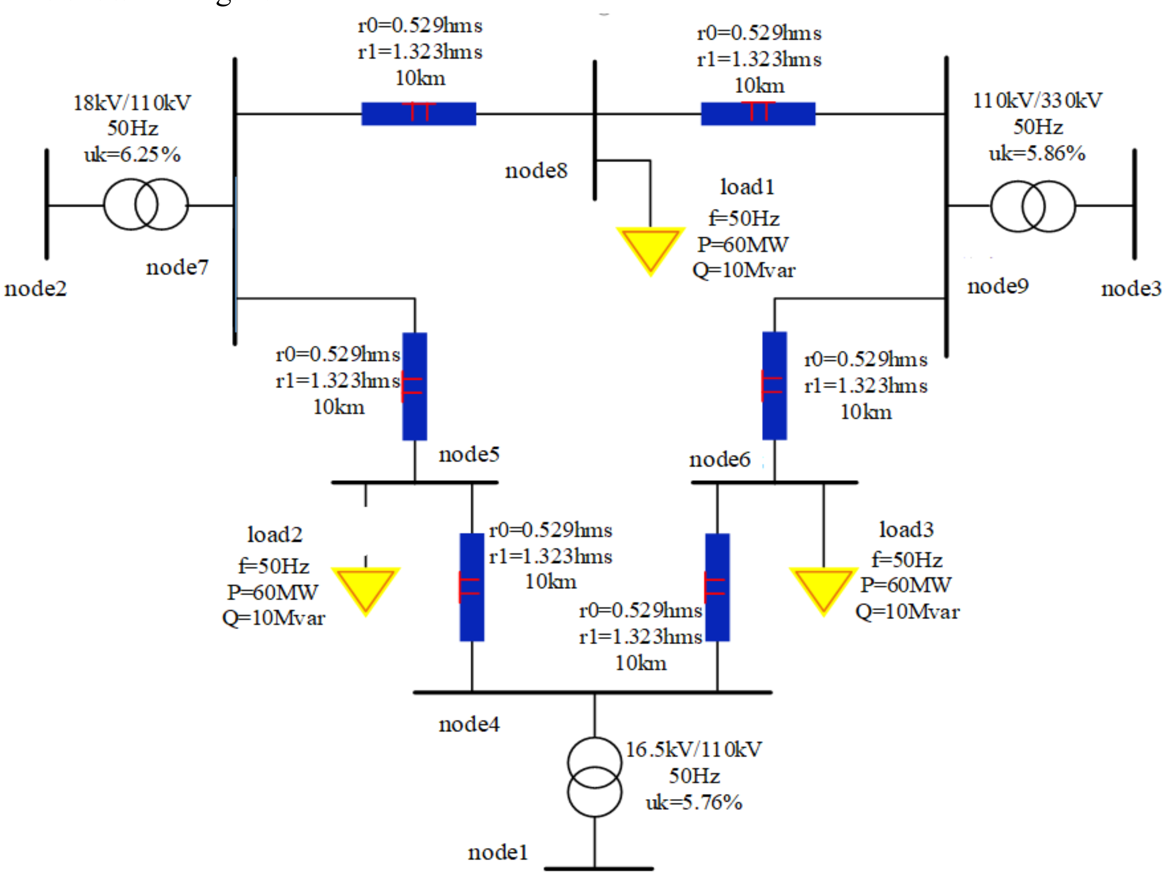

Fig. 3 The established model of the hybrid power system.

3 Interaction effect analysis

The initial values of FHTGU are $(x_{10}, x_{20}, x_{30}, x_{40}, x_{50})^T$=(0.1, 0.2, 0.3, 0.4, 0.5)^T. Model parameters of FHTGU are extracted from *Nazixia* hydropower station, which are listed in Tab. 2.

3.1 Method validation

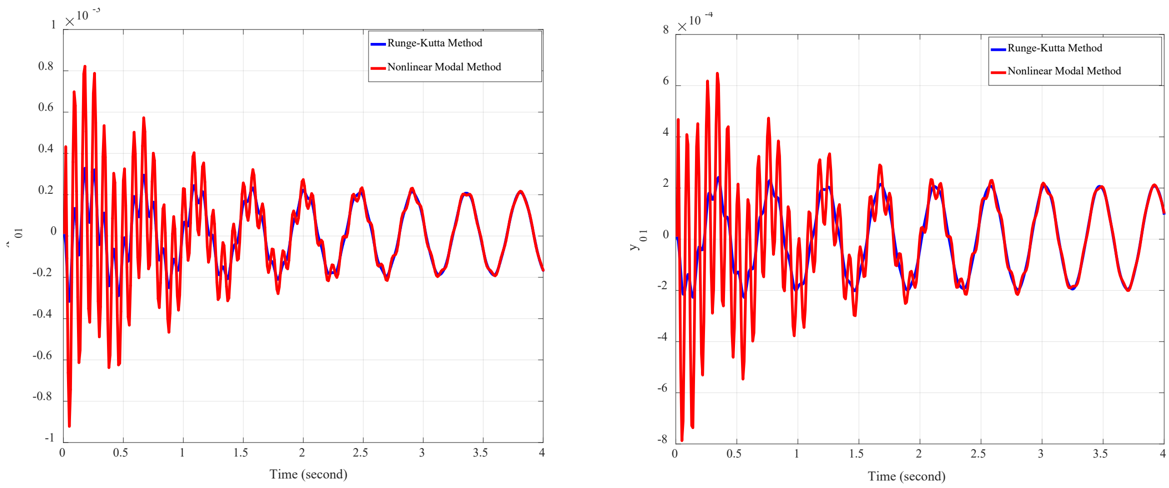

(a) Centroid derivation of the generator rotor in x-axis (b) Centroid derivation of the generator rotor in y-axis

Fig. 4 Centroid derivation responses of the generator rotor with modal series and Runge-Kutta methods. Symbols x_{01} and y_{01} refer to the centroid derivations of the generator rotor in x-axis and y-

axis. The unit is millimeter for x_{01} and y_{01}. The blue line refers to the derivation responses of the generator rotor solved by Runge-Kutta method. The red line refers to the derivation responses of the generator rotor solved by nonlinear modal method.

From Fig. 4, the dynamic responses of the generator rotor with the two methods show a big difference when time is less than 2.5 seconds. While time is larger than 2.5 seconds, the time waveforms are completely coincident with each other. In other words, the modal series method manifests the dynamic response behaviors of the FHTGU accurately and quickly. Hence, the nonlinear modal series method is appropriate in modeling the dynamic characteristics of FHTGU.

Tab. 2 *Nazixia* hydropower station parameters.

Component	Parameter	Symbol	Value	Unit
Penstock	Material: Steel			
	Length	L	216	m
	Diameter	D_L	5	m
Hydro-turbine	Type: HLD294-LJ-178			
	Maximum head	H_{max}	113.5	m
	Rated head	H_{rated}	103	m
	Rated power	P_{rated}	29000	Kw
	Rated speed	n_{rated}	428.6	r/min
	Rated flow	Q_{rated}	32.86	m^3/s
	Zero load flow	Q_{nl}	4.5	m^3/s
	Guide vane opening	Y_{max}	205	mm
	Zero load guide vane opening	Y_{nl}	21%	--
	the mass of the hydro-turbine runner	m_2	1.1×10^4	kg
	the damping coefficient	c	6.5×10^4	N·s/m
	the bearing stiffness of the runner	k_2	6.5×10^7	N/m
	the eccentric mass of the runner	e_2	0.0005	m
	the initial phase	θ_0	0.8	rad/s
	moment of inertia for the runner	J_2	3.5×10^6	kg·m^2
	command signal	s	10^{-5}	--
Generator	Type: FS29-14/4000			
	Active power	$P_{e\text{-}rated}$	29	MW
	Direct axis synchronous reactance	X_d	0.9736	Ω
	Direct axis transient reactance	$X_{d'}$	0.2836	Ω
	Quadrature synchronous axis reactance	X_q	0.6169	Ω
	Quadrature transient axis reactance	$X_{q'}$	0.6169	Ω
	Rated terminal voltage	$U_{S\text{-}rated}$	6.3	kV
	Damping factor	D_t	5	--
	Transient time constant of axis	T_{d0}	5.4	s
	Mass of the rotor for the generator	m_1	1.5×10^4	kg
	the bearing stiffness of the rotor	k_1	8.5×10^7	N·s/m
	the eccentric mass of the rotor	e_1	0.0005	m
	moment of inertia for the rotor	J_1	7.9×10^6	kg·m^2
Governor	Type: CVT-80-4 (PID)			

Permanent speed droop	b_p	0~10%	--
proportional gain	k_p	0.5~20	s
integral gain	k_i	0.05~10	s
differential gain	k_d	0~5	s

3.2 Eigenvalue and linear participation factor analyses

Based on section 2.3, the eigenvalue of each oscillation mode is defined as

$$\lambda_j = \sigma_j + i\chi_j , \tag{14}$$

where variables σ and χ refer to the damping coefficient and angular frequency, respectively. The damping ratio ζ is

$$\zeta = \frac{-\sigma}{\sqrt{\sigma^2 + \chi^2}} , \tag{15}$$

and its oscillation frequency f is

$$f = \frac{\chi}{2\pi} . \tag{16}$$

When the damping ratio is larger than zero, the FHTGU operates in a stable oscillation mode. On the contrary, the FHTGU operates in an unstable mode as the damping ratio is less than zero. Here, the frequency of oscillation modes and damping ratio is obtained based on Eqs. (17-19), which are shown in Tab. 3.

Tab. 3 Eigenvalue analysis of FHTGU.

State variable	mode	Eigenvalue	Frequency/Hz	Damping ratio
x_{01}, y_{01}	$\lambda_{1,2}$	$-1.25\pm1.9153i$	0.3050	0.5465
v_x, v_y	$\lambda_{3,4}$	$-1.25\pm1.8860i$	0.3003	0.5525
z	λ_5	0	0	--

From Tab. 3, there are two pairs of complex conjugate roots $\lambda_{1,2}$ and $\lambda_{3,4}$. The damping ratio corresponding to eigenvalues is greater than zero, confirming that the FHTGU operates in a stable condition. The corresponding oscillation frequency and damping ratio are 0.3 and 0.55, respectively. In addition, from section 2, we obtain that the velocities (v_x, v_y) is solved from the first-order derivative of deviations (x_{01}, y_{01}). Hence, the same oscillation frequency and damping ratio to the state variables (x_{01}, y_{01}) and (v_x, v_y) verify the correctness of the calculation results of Tab. 3.

The participation factor is divided into the linear participation factor ($\sigma_{ij}=u_{ij}v_{ji}$, see Eq. (16)) and single mode nonlinear participation factor ($P2_{ij}$, see Eq. (16)). The linear participation factor σ_{ij} describes the contribution of mode λ_j to state variable x_i when the system is excited by a small perturbation. The single mode nonlinear participation factor $P2_{ij}$ denotes the second-order nonlinear interaction between j-th mode and i-th state variable [10]. Tab. 4 shows the linear participation factor of the FHTGU. Tab. 5 presents the single mode nonlinear participation factor in state variables.

Tab. 4 Amplitude of the linear participant factor.

State variable	mode 1, 2	mode 3, 4	mode 5
x_{01}	0.027531	0	0.004602

y_{01}	0.061004	0	0.021956
v_x	0.050025	0	0
v_y	0	0.049943	0
z	0	0	0.100020

Tab. 5 Amplitude of the single mode nonlinear participation factor

State variable	mode 1	mode 2	mode 3	mode 4	mode 5
x_{01}	0.12	0.26	0.9	0.01	0.06
y_{01}	0.23	0.4	0.03	0.01	0.72
v_x	0.58	0.47	0.03	0.13	0.18
v_y	0.01	0.3	0.03	0.98	0.22

From Tab. 4, modes 1 and 2 are mainly associated with the state variables y_{01} and v_x, respectively. Modes 3 and 4 are both related to v_y, and mode 5 has a great influence on the state variable z. From Tab. 5, modes 1, 2, 3, 4 and are both affected by the state variable x_{01}, y_{01}, v_x, and v_y. Moreover, variable v_x makes a major contribution in deciding modes 1 and 2. Models 3, 4 and 5 are mainly affected by variable x_{01}, v_y, and y_{01}, respectively.

In light of the above analysis, the amplitude of nonlinear participation factor $P2_{ij}$ (Tab. 5) are very different compared with the linear participation factor (Tab. 4), which is caused by the second nonlinear interaction term (part of Eq. (16)). Combining with the verification analysis of Fig. 1, the single mode nonlinear participation factor can better capture the dynamic behaviors of FHTGU in the modal series theory.

3.3 Nonlinear Modal Interaction Index Analysis

In Eq. (12), the second order modal time response expressed by $K^i_{kl}e^{(\lambda_k+\lambda_l)t}$ consists of two indexes, including K^i_{kl} and $e^{(\lambda_k+\lambda_l)t}$. Index K^i_{kl} determines the maximum amplitude of the second order modal time response. The time constant (T_{kl}=－$1/real(\lambda_k+\lambda_l)$) of $e^{(\lambda_k+\lambda_l)t}$ determines the duration time from fluctuation to stable with respect to state variables. The larger the value K^i_{kl} is, the more pronounced influence of interacting second order mode will be. The larger the time constant T_{kl} is, the longer the influence of this mode will last [12]. In light of the above analysis, symbol $I2^i_{kl}$ is defined as a measure index for the influences of interaction modes to capture both amplitude and duration effects of interacting modes, which is

$$I2^i_{kl} = \left| \frac{K^i_{kl}}{\mathrm{Re}\left(\lambda_k + \lambda_l\right)} \right|. \tag{17}$$

From Eq. (17), index $I2^i_{kl}$ can quantify the intensity of each mode interaction to facilitate the investigation of dominant nonlinear interaction modes. In addition, results of the second order modal series simulation indicate that the nonlinear system response contains multiple nonlinear interaction modes. In other words, there are more interactive modes except for the above 5 detectable eigenvalues from the linear model in the nonlinear system responses, such as $\lambda_{i,j}$=λ_i+λ_j. The interaction intensity of modes on state variables for the Francis hydro-turbine generator unit is shown in Fig. 5.

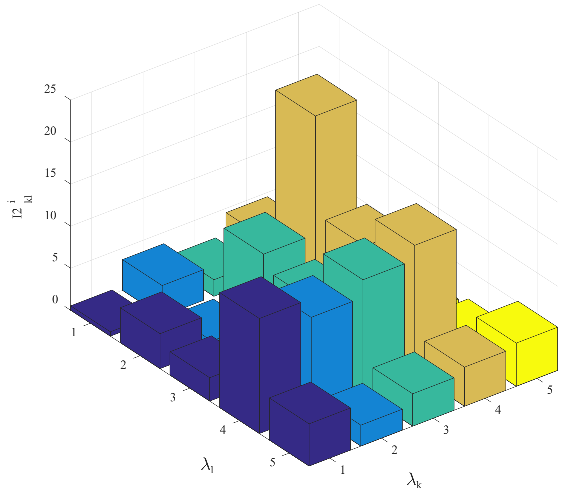

(a) Mode interaction of x_{01}

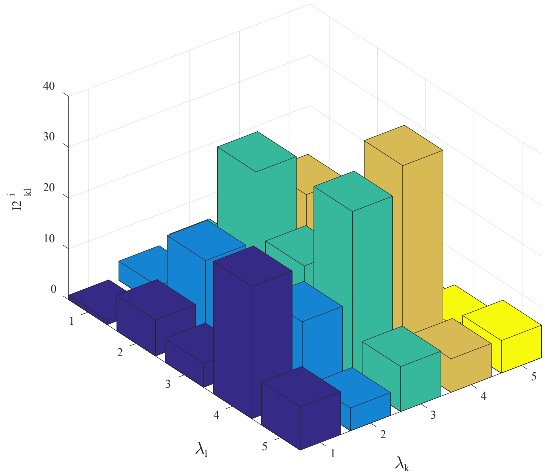

(b) Mode interaction of y_{01}

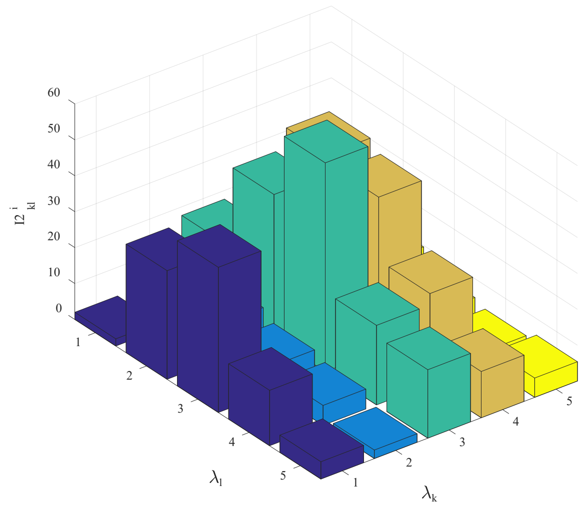

(a) Mode interaction of v_x

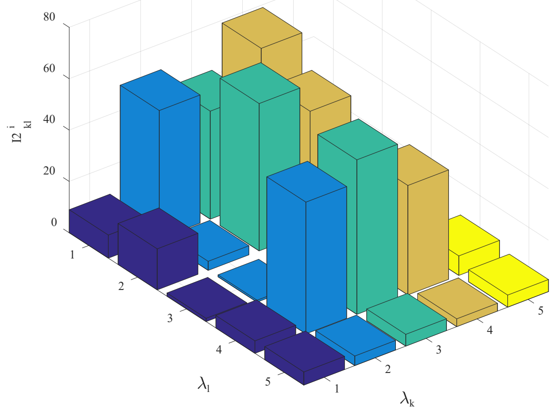

(b) Mode interaction of v_y

Fig. 5 The interaction intensity of modes on state variables for the Francis hydro-turbine generator unit. λ_l and λ_k are the eigenvalues of Francis hydro-turbine generator unit. $I2^i_{kl}$ is the interaction intensity of modes λ_l and λ_k on state variables.

From Fig. 5(a) and Fig. 5(b), $\lambda_{k=1,2,3,l=4}$ and $\lambda_{k=4,l=2,3,4}$ are the dominant nonlinear interaction modes for variable x_{01}. $\lambda_{k=1,l=4}$ and $\lambda_{k=2,3,4,l=2,3,4}$ are the dominant nonlinear interaction modes for variable y_{01}. The dominant nonlinear interaction modes play a major role in deciding the dynamic behavior of FHTGU. According to the definition of $I2^i_{kl}$, the amplitude and duration of dynamic behavior to state variables are larger and longer when index values of these dominant interaction modes are greater. Here, $\lambda_{k=4,l=2,3,4}$ is the maximum value corresponding to the interaction intensity between x_{01} and y_{01}. From Fig. 5(c) and Fig. 5(d), $\lambda_{k=1,l=2,3,4}$ and $\lambda_{k=3,4,l=1,2,3,4,5}$ play a leading role in variable v_x, so do $\lambda_{k=2,l=1,4}$ and $\lambda_{k=3,4,l=1,2,4}$ in velocity of rotor axis in Y-direction v_y. Comparing Fig. 5(d) with the others, it can be noted that the dominant interaction modes have altered with different state variables. Additionally, such the strongest interaction modes as $\lambda_{k=2,4,l=1}$ and $\lambda_{k=3,l=2,4}$ imply that velocity of rotor axis in Y-direction v_y has a great influence on FHTGU.

Through the above analysis, the interaction of these dominant modes makes the dynamic behavior of FHTGU more complicated. Therefore, the approximate equation of mode is obtained by selecting the dominant mode of state variables to further capture the dynamic characteristics of FHTGU. For variable v_x, the approximate expression of dominant mode is defined as

$$v_x(t)=\sum_{j=1}^{5}u_{3j}\left(y_{j0}-\left(\sum_{k=1}^{5}\sum_{l=1}^{5}h2_{kl}^{j}y_{k0}y_{l0}\right)\right)e^{\lambda_j t}+\sum_{j=1}^{5}u_{3j}\sum_{k=1}^{1}\sum_{l=2}^{4}h2_{kl}^{j}y_{k0}y_{l0}e^{(\lambda_k+\lambda_l)t}+\sum_{j=1}^{5}u_{3j}\sum_{k=3}^{4}\sum_{l=1}^{5}h2_{kl}^{j}y_{k0}y_{l0}e^{(\lambda_k+\lambda_l)t}. \quad (18)$$

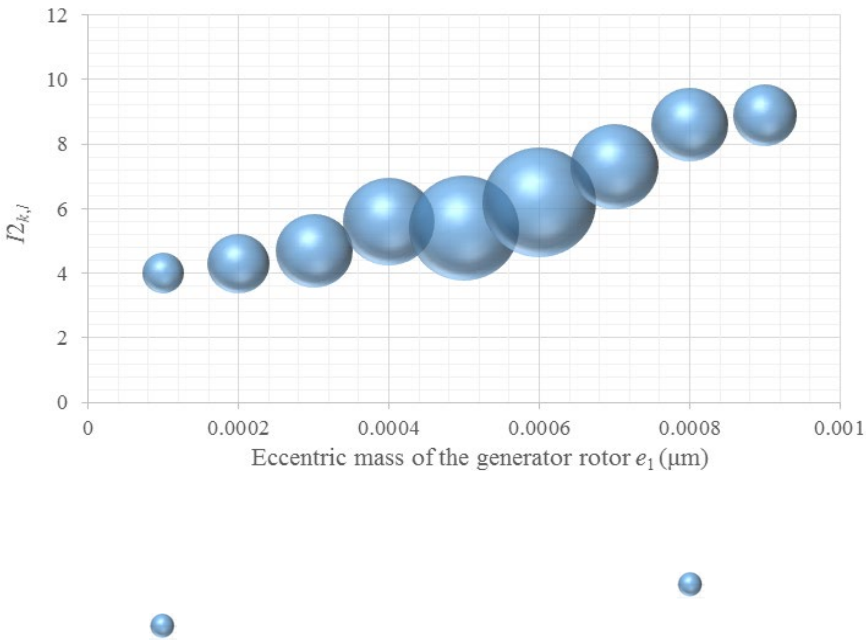

The eccentric mass of the generator rotor e_1 is a general fault for FHTGU. Here, an example of this fault corresponds to the nonlinear interaction index $I2_{k,l}$ of interaction mode is investigated (see Fig. 3). From Fig. 6, the related action of the general mode $\lambda_{k=1,l=5}$ gradually increases with the increasing value of e_1. The related action of the dominant mode $\lambda_{k=1,l=2}$ increases and then decreases with the increasing of e_1, so that there is a maximum point. The ratio of the related action of modes has a significant difference in the variation range of e_1. It confirms that dominant modes have the most significant influence on the dynamic behaviors of FHTGU. It is illustrated that adjusting this fault can make the running FHTGU as quickly as possible to reach a stable state.

3.4 Vibration characteristics of the generator rotor and hydro-turbine runner

In section 3.2, the nonlinear interaction index of interaction modes were investigated. Model parameters are adopted from Tab. 2. In order to clearly reveal the difference of the vibration characteristics between the generator rotor and the hydro-turbine runner, a comparison is performed to show the difference of the vibration characteristics for the generator rotor and hydro-turbine runner, as shown in Fig. 7.

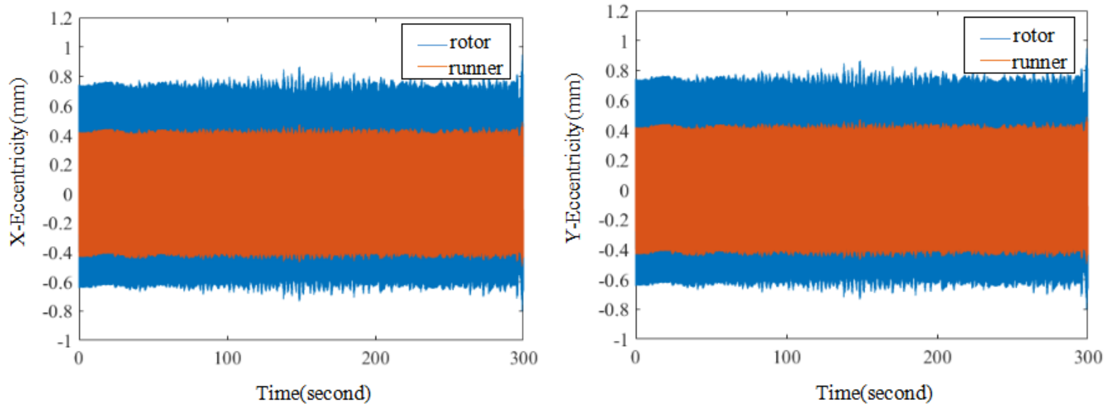

(a) The vibration characteristics in X-direction (b) The vibration characteristics in X-direction

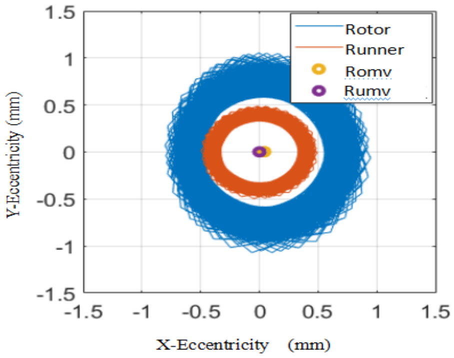

(c) Axis orbit of the generator rotor and hydro-turbine runner

Fig. 7 The vibration characteristics for the generator rotor and hydro-turbine runner. Variables Romv and Rumv refer to the average value of the rotor and runner.

As shown in Fig. 7(a, b), the responses of the generator rotor and the hydro-turbine runner are compared in X-direction and Y-direction. The vibration amplitude of the generator rotor is higher than that of the hydro-turbine runner. It is worth noting that the rotor's vibration amplitude fluctuates within the range of ±0.4mm, and the maximum amplitude of the rotor in the negative direction X is only 0.2mm higher than the maximum amplitude of the runner. Furthermore, by comparing the axis orbit of the generator rotor and hydro-turbine runner shown in Fig. 7(c), it is found that the rotor's vibration range within 300 seconds is larger than that of the runner. By comparing with the runner's vibration trajectory, the rotor's vibration trajectory is offset in the positive X-direction, and the mean value of the rotor is larger, indicating that the center of the rotor's axis trajectory is offset in the positive X-direction.

3.5 Vibration characteristics affected by the wind generation system

To investigate the vibration characteristics of FHTGU affected by the wind generation system, the wind speed model established in Section 3.1 is adopted, which is shown in Fig. 1. This model consists of four types wind speed: basic wind, gradually increasing wind speed, gradually decreasing wind speed and gust wind. To reflect the influence of different wind speed conditions on the rotor motion, 6 typical wind speeds (i.e. WS1-WS6,) are extracted in the time scale of 10 seconds, and the vibration of the rotor in the X-direction and Y-direction under the above 6 characteristic wind speeds is used, as shown in Fig. 8. The axis orbit of FHTGS affected by 6 typical wind speeds are shown in Fig. 9.

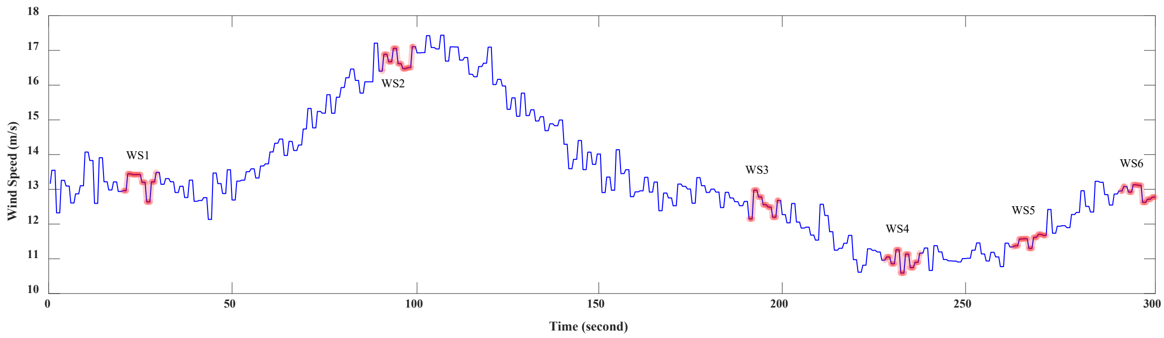

Fig. 8 Six typical wind speed disturbance. WS1 to WS6 are selected to analyze the vibration characteristics of the hydroelectric generating system;

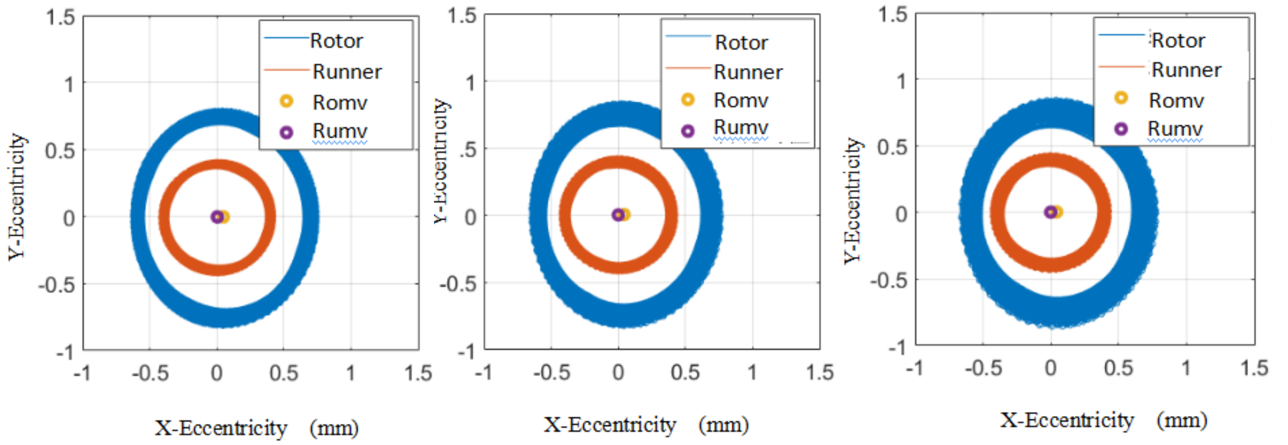

(*a*) Axis orbit affected by WS1 (*b*) Axis orbit affected by WS2 (*c*) Axis orbit affected by WS3

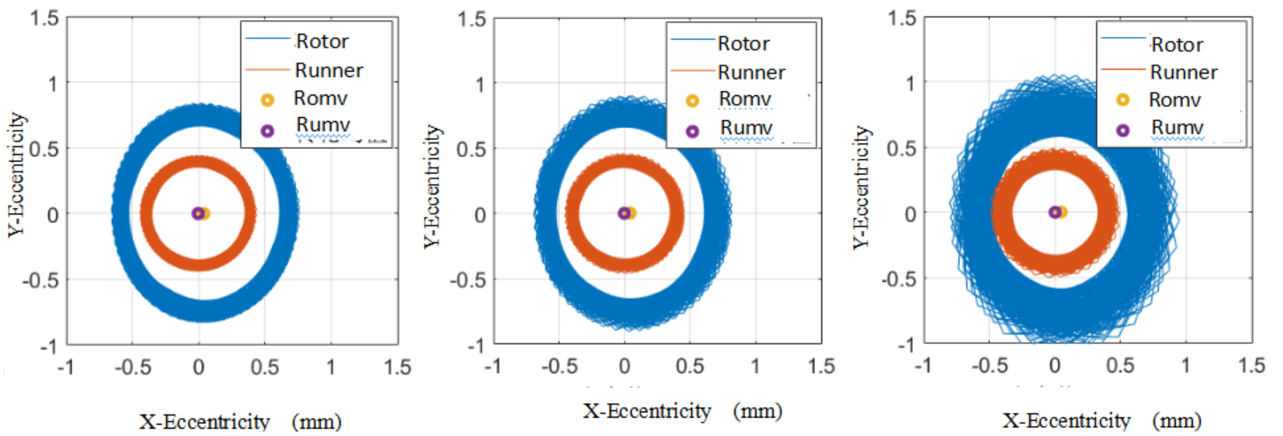

(*d*) Axis orbit affected by WS4 (*e*) Axis orbit affected by WS5 (*f*) Axis orbit affected by WS6

Fig. 9 Comparison of the axis orbit of FHTGS affected by 6 typical wind speeds. Variables Romv and Rumv refer to the average value of the rotor and runner.

From Fig. 9(a-e), the axis track of the runner is located in the inner side of the rotor track. For Fig. 7(f), there is a small part of coincidence on the left side for the generator rotor and hydro-turbine runner in the X-axis. Obviously, the dynamic orbit of the runner is close to a circle, and the average value shows that the trajectory of the center is closer to (0, 0), about 4.33 mm. For the generator rotor, the vibration amplitude of the generator rotor is greater than the negative direction in the X-axis, which lead to the trajectory looks relatively flat. The left part of the axis of the trajectory under this role also shift to the right in the X-axis, which is about 3.31 mm. Interestingly, for the wind disturbance WS6, the motion trajectory of the rotor and runner covers a wider range, indicating that the vibration and deviation of the shafting are serious at this time.

In the following, the influence of different wind capacity ratios on the shafting stability of the FHTGU is investigated using eight indexes, i.e. the mean value in the X-direction and Y-direction, the maximum mean value in the positive X-direction and positive Y-direction, the maximum mean value in the negative X-direction and negative Y-direction, the variance in the X-direction and Y-direction. The values of these indexes are obtained by accumulating and averaging the maximum values in each vibration period in 300 seconds. The obtained results of these indexes with different hydro-wind capacity ratio are shown in Table 5 and Table 6.

Tab. 5 The stability indexes of the generator rotor with different hydro-wind capacity ratio.

Index of rotor stability (10-3 mm)	X mean value	Y mean value	X^+mean value	Y^+mean value	X^-mean value	Y^-mean value	X variance	Y variance
R=1.25	43.552	3.481	758	824	-645	-822	2.304	3.698
R=1	43.297	3.471	753	815	-639	-815	1.097	1.595
R=0.75	43.066	3.384	750	813	-639	-812	0.518	0.747
R=0.5	42.556	4.228	747	811	-638	-810	0.204	0.243
R=0.25	42.345	4.164	745	809	-636	-810	0.127	0.119

Index of runner stability (10-3 mm)	X mean value	Y mean value	X^+mean value	Y^+mean value	X^-mean value	Y^-mean value	X variance	Y variance
R=1.25	0.393	1.799	432	431	-430	-431	0.337	3.698
R=1	0.331	1.818	428	428	-426	-428	0.258	1.595
R=0.75	0.186	1.789	427	427	-426	-426	0.518	0.747
R=0.5	-0.183	2.247	425	426	-426	-426	0.204	0.243
R=0.25	-0.339	2.228	425	425	-425	-424	0.127	0.119

From Tab. 3, the mean value in the X-direction, the maximum mean value in the positive X-direction and positive Y-direction, the maximum mean value in the negative X-direction and negative Y-direction, the variance in the X-direction and Y-direction increase with the increase of wind power, which leads to the intensification of shafting vibration. This is because when the wind power of the complementary power generation system increases, the compensation power of the hydropower needed also increases. The increase of flow brings greater impact on the shafting, resulting in the decline of the shafting stability. The only exception is the index of the mean values in the Y-direction, which are 0.5, 0.25, 1.25, 1, and 0.75 in order of the ratio from large to small. For the runner, as shown in Table 4, the mean values in the Y-direction from large to small are 0.5, 0.25, 1, 1.25 and 0.75, respectively. In addition, with the increase of the hydro-wind capacity ratio, the index of stability also increases gradually. However, such an increase trend does not show a linear rule, especially in the process of increasing the ratio from 1 to 1.25, the range of stability index growth is far higher than that of other adjacent powers.

4 Conclusions

In this study, the nonlinear modal theory is successful applied to FHTGU, and the interaction effect of nonlinear modes are investigated. Three main conclusions are obtained. First, by comparing the simulation results solved by Runge-Kutta method with the closed-form solution obtained by the modal series method with the time domain simulation results, the modal series method can well reflect the dynamic characteristics of HTGU. Second, the nonlinear correction term in the nonlinear participation factor of the single mode changes the interaction effect between modes and state variables. Third, the dominant nonlinear interaction mode corresponds to different dominant nonlinear interaction modes by analyzing the nonlinear modal interaction index different. Finally, the vibration characteristics affected by the wind generation system are investigated. In addition, the HTGU can be better understood and analyzed based on nonlinear modal analysis, and the valuable frequency domain information is provided for designing FHTGU's controller to improve its operating stability.

Acknowledgments

This research is supported by the Fundamental Research Funds for the Northwest A&F University (No. /Z1090220172), the scientific research foundation of the Natural Science Foundation of Shaanxi Province of China (2019JLP-24), Shaanxi Science and Technology Innovation Team, and Water Conservancy Science and Technology Program of Shaanxi Province (2018slkj-9).

Supplementary Note

Unbalanced hydraulic forces

The force of water acting on the runner blade is [27]

$$R = \rho W_{ma} \Gamma_a , \tag{1}$$

where W_{ma} is the average value of the relative velocity around the blade; Γ_a is the average circulation, $\Gamma_a = \pi D_2 V_{u2}$.

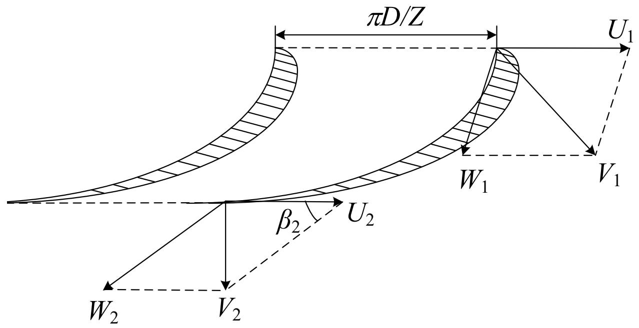

Fig. 1 Velocity triangle of a hydro-turbine generator unit. Symbols D and Z refer to the runner diameter at the inlet and the number of the hydro-turbine blades, respectively. Symbols U_1, V_1 and W_1 refer to the convected velocity, absolute velocity, and relative velocity for the blade at the inlet, respectively. Symbols U_2, V_2 and W_2 refer to the convected velocity, absolute velocity, and relative velocity for the blade at the outlet, respectively.

Based on Kutta-Joukowski theorem, the component of the asymmetric radial force is [27, 28]

$$P_m = \frac{C_y \gamma F W_m^{\ 2} \cos\left(\beta_m - \lambda\right)}{2g \cos\lambda}, \tag{2}$$

where C_y, F and β_m are the lift coefficient of the runner blade, the maximum area of the runner blade and the angle between the average relative velocity and peripheral direction, respectively. W_1 is the average velocity for the blade at the inlet, $W_1=4Q/\pi D_1^2$. W_2 is the average velocity for the blade at the outlet. W_m is the geometric mean velocity of W_1 and W_2, $W_m=sqrt(W_1 \times W_2)$. γ is the liquid weight around the runner blade.

When the Reynolds number changes in the interval (10^4, 10^6), the resistance coefficient C_x and the radio λ are expressed as [28]

$$\begin{cases} C_x = 2\sin(\dfrac{\arcsin C_y}{2})^2 \\ \lambda = \arctan\dfrac{C_x}{C_y} = \arctan\dfrac{2\sin(\dfrac{\arcsin C_y}{2})^2}{C_y} \end{cases}. \tag{3}$$

The velocity at point 1 or 2 (see Fig. 2a) is reduced to the relative velocity expressed by symbol W, the convected velocity represented by U, and the absolute velocity of V. β is the angle between the relative velocity W and the velocity U. α is the angle between the absolute velocity V and the velocity U. Subscript 1 refers to the velocities at the runner inlet, and the subscript 2 refers to the velocities at the runner outlet.

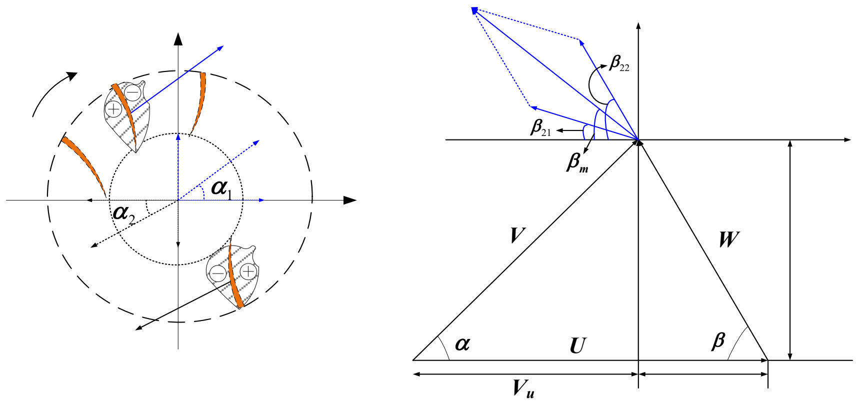

(a) Unbalanced hydraulic forces of blades 1 and 13. (b) Velocity triangle of the blade.

Fig. 2 Francis turbine runner and the velocity triangle of the blade. Variables U, V, and W are the convected velocity, absolute velocity, and relative velocity for the blade at the inlet, respectively; β is the angle between W and U; α is the angle between V and U; Subscripts 1 and 2 refer to the runner inlet and outlet points. P_{m1} and P_{m13} are both the unbalanced hydraulic forces of a pair of runner blades (Number 1 and 13); α_1 and α_{13} are the position angles of blades 1 and 13, respectively; β_{m} is the angle between the average relative velocity (W_m) and convected velocity (U); W_m is the average relative velocity of the turbine runner.

The relative flow velocity at the inlet is

$$W_1 = \frac{V_{m1}}{\sin\beta_1} = \frac{Q}{\pi s_1 b_0 D_1 \sin\beta_1}. \tag{4}$$

where Q is the hydro-turbine flow; s_1 is the excretion coefficient at point 1; b_0 is the height of the blade; β_1 is the angle between W_1 and U_1 (see Fig. 1). D_1 is the diameter of the hydro-turbine runner at the inlet. From Fig. 2b, the relative flow velocity at the outlet is

$$\begin{cases} W_2 = \dfrac{V_{m2}}{\sin\beta_2} \\ V_{m2} = \dfrac{Q}{F_2} = \dfrac{Q}{s_2 \pi D_2^{\,2}} \end{cases}. \tag{5}$$

Let us define the direction of the convected velocity as the x-axis (see Fig. 2b). Then, the coordinates of the velocity W_1, W_2, and W_{m} are ($W_1 cos\beta_1$, $W_1 sin\beta_1$), ($W_2 cos\beta_2$, $W_2 sin\beta_2$), and ($W_1 cos\beta_1+W_2 cos\beta_2$, $W_1 sin\beta_1+W_2 sin\beta_2$), respectively. Hence, the absolute value of W_{m} is

$$|W_m| = \sqrt{W_1^2 + W_1^2 + 2W_1W_2\cos(\beta_1-\beta_2)}. \tag{6}$$

The angle between the velocity W_{m} and the convected velocity is

$$\beta_m = \arcsin\frac{W_1 \sin\beta_1 + W_2 \sin\beta_2}{|W_m|}. \quad (7)$$

With Eq. (6) and Eq. (7), Eq. (23) is detailed as

$$P_m = \frac{\gamma C_y F \cos(\beta_m - \lambda)}{2g\cos\lambda}\left(W_1^2 + W_1^2 + 2W_1W_2\cos(\beta_1 - \beta_2)\right). \quad (8)$$

If the initial angle of the blade is α_0, then the position angle of the blade at time t is

$$\alpha = \alpha_0 + \omega t \quad (9)$$

The component forces of P_m in the X-direction and Y-direction are

$$\begin{cases} P_x = P_m \cos\alpha \\ P_y = P_m \sin\alpha \end{cases}. \quad (10)$$

Theoretically, the water flowing in the turbine runner is the axisymmetric spatial flow. In actual situations, there are radial asymmetry forces relative to the center of turbine runner due to the manufacturing deviations of the blades at the outlet edges. For example, assuming a pair of runner blades (numbered 1 and 13) exists the manufacturing deviation.

Let us define the relative velocity at the outlet edge as W_{21}, and define the angle between the relative velocity and the circumferential direction of blade 1 as β_{21} (see Fig. 2b). Also, let us define the relative velocity for another blade is W_{22}, and define the angle between the relative velocity and the circumferential direction of convected velocity for the blade is β_{22} (see Fig. 2b). Let us define the angle between the velocity W_{21} and the convected velocity as β_{m1}. In light of Eqs. (22-31), the expression of β_{m1} is

$$\beta_{m1} = \arcsin\frac{W_1 \sin\beta_1 + W_{21} \sin\beta_{21}}{|W_{m1}|}. \quad (11)$$

Similarly, if we define the angle between the velocity W_{22} and the convected velocity for other blades as β_{m2}, then we can derive as

$$\beta_{m2} = \arcsin\frac{W_1 \sin\beta_1 + W_{22} \sin\beta_{22}}{|W_{m2}|}. \quad (12)$$

In light of the above analysis, the unbalanced hydraulic forces (see Fig. 2b) are

$$\begin{cases} P_x = P_{m1}\cos\alpha_1 - P_{m13}\cos\alpha_{13} = \dfrac{\gamma C_y F|\cos\alpha|}{2g\cos\lambda}\left[A_1\cos(\beta_{m1} - \lambda) - A_2\cos(\beta_{m2} - \lambda)\right] \\ P_y = P_{m1}\sin\alpha_1 - P_{m13}\sin\alpha_{13} = \dfrac{\gamma C_y F|\sin\alpha|}{2g\cos\lambda}\left[A_1\cos(\beta_{m1} - \lambda) - A_2\cos(\beta_{m2} - \lambda)\right] \end{cases}, \quad (13)$$

where $\begin{cases} A_1 = \dfrac{Q^2}{\left(s_1\pi D_1^2\sin\beta_1\right)^2} + \dfrac{Q^2}{\left(s_2\pi D_2^2\sin\beta_{21}\right)^2} + \dfrac{2Q^2\cos(\beta_1 - \beta_{21})}{s_1s_2\pi^2D_1^2D_2^2\sin\beta_1\sin\beta_{21}} \\ A_2 = \dfrac{Q^2}{\left(s_1\pi D_1^2\sin\beta_1\right)^2} + \dfrac{Q^2}{\left(s_2\pi D_2^2\sin\beta_{22}\right)^2} + \dfrac{2Q^2\cos(\beta_1 - \beta_{22})}{s_1s_2\pi^2D_1^2D_2^2\sin\beta_1\sin\beta_{22}} \end{cases}.$

References

[1] Rehman S, Al-Hadhrami LM, Alam MM. Pumped hydro energy storage system: A technological review. Renewable & Sustainable Energy Reviews. 2015;44:586-598.

[2] Wu QQ, Zhang LK, Ma ZY. A model establishment and numerical simulation of dynamic coupled hydraulic-mechanical-electric-structural system for hydropower station. Nonlinear Dynamics. 2017;87:459-474.

[3] Behrens P, van Vliet MTH, Nanninga T, Walsh B, Rodrigues JFD. Climate change and the vulnerability of electricity

generation to water stress in the European Union. Nature Energy. 2017;2(8), DOI: 10.1038/nenergy.2017.114.

[4] Beevers D, Branchini L, Orlandini V, De Pascale A, Perez-Blanco H. Pumped hydro storage plants with improved operational flexibility using constant speed Francis runners. Applied Energy. 2015;137:629-637.

[5] M'Zoughi F, Bouallegue S, Garrido AJ, Garrido I, Ayadi M. Stalling-Free Control Strategies for Oscillating-Water-Column-Based Wave Power Generation Plants. Ieee Transactions on Energy Conversion. 2018;33:209-222.

[6] Rezghi A, Riasi A. The interaction effect of hydraulic transient conditions of two parallel pump-turbine units in a pumped-storage power plant with considering "S-shaped" instability region: Numerical simulation. Renewable Energy. 2018;118:896-908.

[7] Yilmaz IH, Mwesigye A. Modeling, simulation and performance analysis of parabolic trough solar collectors: A comprehensive review. Applied Energy. 2018;225:135-174.

[8] Pariz N, Shanechi HM, Vaahedi E. Explaining and validating stressed power systems behavior using modal series. IEEE Trans Power Syst. 2003;18:778-785.

[9] Shanechi HM, Pariz N, Vaahedi E. General Nonlinear modal representation of large scale power systems. IEEE Trans Power Syst. 2003;18:1103-1109.

[10] Martinez I, Messina AR, Barocio E. Perturbation analysis of power systems: effects of second- and third-order nonlinear terms on system dynamic behavior. Electric Power Systems Research. 2004;71:159-167.

[11] Zou ZY, Jiang QY, Cao YJ, Wang HF. Application of the normal forms to analyze the interactions among the multi-control channels of UPFC. Int J Electr Power Energy Syst. 2005;27:584-593.

[12] Khatibi M, Shanechi HM. Using a modified Modal Series to analyse weakly nonlinear circuits. International Journal of Electronics. 2015;102:1457-1474.

[13] Sajjadi SS, Pariz N, Karimpour A, Jajarmi A. An off-line NMPC strategy for continuous-time nonlinear systems using an extended modal series method. Nonlinear Dynamics. 2014;78:2651-2674.

[14] Li Y, Lin L, Zhang X, Cheng GX. Comparison of various sound models for predicting transmission loss of compressor mufflers based on the modal series expansion method. Hvac&R Research. 2012;18:539-548.

[15] Jajarmi A, Hajipour M. An efficient parallel processing optimal control scheme for a class of nonlinear composite systems. Acta Mathematica Scientia. 2017;37:703-721.

[16] Naghshbandy AH, Shanechi HM, Kazemi A, Pourfar I. Study of fault location effect on the inter-area oscillations in stressed power systems using modal series method. Electrical Engineering. 2010;92:17-26.

[17] Zhang H, Li WJ, Ding HH, Luo PC, Wan XJ, Hu WB. Nonlinear Modal Analysis of Transient Behavior in Cascade DC-DC Boost Converters. International Journal of Bifurcation and Chaos. 2017;27(9). DOI: 10.1142/S0218127417501401.

[18] Pennacchi P, Chatterton S, Bachschmid N, Pesatori E, Turozzi G. A model to study the reduction of turbine blade vibration using the snubbing mechanism. Mechanical Systems and Signal Processing. 2011;25:1260-1275.

[19] Perez-Diaz JI, Frank Burke ML. Integration of fast acting energy storage systems in existing pumped‐storage power plants to enhance the system's frequency control. Wiley Interdisciplinary Reviews: Energy and Environment, 2020, 9: e367.

[20] Martínez-Lucas G, Perez-Diaz JI, Chazarra M., et al. Risk of penstock fatigue in pumped-storage power plants operating with variable speed in pumping mode. Renewable Energy, 2019, 133: 636-646.

[21] Li HH, Chen DY, Zhang H, Wu CZ, Wang XY. Hamiltonian analysis of a hydro-energy generation system in the transient of sudden load increasing. Applied Energy. 2017;185:244-253.

[22] Xu BB, Chen DY, Zhang H, Zhou R. Dynamic analysis and modeling of a novel fractional-order hydro-turbine-generator unit. Nonlinear Dynamics. 2015;81:1263-1274.

[23] Zhang LK. Nonlinear dynamic analysis of shaft system for hydroelectric generating set. Dalian University Of Technology, 2014. (In Chinese)

[24] Zeiner-Gundersen DH. A novel flexible foil vertical axis turbine for river, ocean, and tidal applications. Applied

Energy. 2015;151:60-66.

[25] Hwang IS, Lee YH, Kim SJ. Optimization of cycloidal water turbine and the performance improvement by individual blade control. Applied Energy. 2009;86(9):1532-1540.

[26] Kakimoto N, Nakanishi A, Tomiyama K. Instability of interarea oscillation mode by autoparametric resonance. IEEE Transactions On Power Systems, 2004;19(4):1961-1970.

[27] Shen ZY. Hydraulic turbine regulating system. China Water & Power Press, 2008, pp. 47. (In Chinese)

[28] Tong WM. Analysis of spindle swing caused by hydraulic unbalance of hydraulic turbine runner. Sichuan Water Power, 1986, 1: 42-46. (In Chinese)

[29] Xu BB, Chen DY, Venkateshkumar M, Xiao Y, Yue Y, Xing YQ, Li PQ. Modeling a pumped storage hydropower integrated to a hybrid power system with solar-wind power and its stability analysis. Applied Energy, 2019, 248, 446-462.